

Current-Driven Dynamics of Magnetic Hopfions

X. S. Wang , A. Qaiumzadeh, and A. Brataas

Center for Quantum Spintronics, Department of Physics, Norwegian University of Science and Technology, NO-7491 Trondheim, Norway



(Received 23 May 2019; published 30 September 2019)

Topological magnetic textures have attracted considerable interest since they exhibit new properties and might be useful in information technology. Magnetic hopfions are three-dimensional (3D) spatial variations in the magnetization with a nontrivial Hopf index. We find that, in ferromagnetic materials, two types of hopfions, Bloch-type and Néel-type hopfions, can be excited as metastable states in the presence of bulk and interfacial Dzyaloshinskii-Moriya interactions, respectively. We further investigate how hopfions can be driven by currents via spin-transfer torques (STTs) and spin-Hall torques (SHTs). Distinct from 2D ferromagnetic skyrmions, hopfions have a vanishing gyrovectore. Consequently, there are no undesirable Hall effects. Néel-type hopfions move along the current direction via both STT and SHT, while Bloch-type hopfions move either transverse to the current direction via SHT or parallel to the current direction via STT. Our findings open the door to utilizing hopfions as information carriers.

DOI: 10.1103/PhysRevLett.123.147203

Topological solitons are of fundamental interest in nonlinear field theories. Additionally, their magnetic realizations are promising candidates as information carriers in the next generation of data storage and processing devices [1,2]. Low-dimensional topological solitonlike textures in ferromagnetic (FM) and antiferromagnetic (AFM) materials, such as 1D magnetic domain walls [3–6], 2D magnetic vortices [7,8], and 2D magnetic skyrmions [9–17], have been extensively studied in recent years.

The existence of 3D topological solitons with stringlike properties has been proposed by Ludvig D. Faddeev [18] as a limit of the Skyrme model [19]. These 3D topological solitons are known as Faddeev-Hopf knots [20] or hopfions, which are classified by a topological charge called the Hopf index [21]. Hopfions have been discussed in many physical systems, such as gauge theories [18,22], cosmic strings [23], ferromagnets [24] (as a special case of dynamical vortex rings), low-temperature bosonic systems [25–27], fluids [28], and liquid crystals [29–31]. Recently, stable magnetic hopfions were numerically predicted in finite-size noncentrosymmetric FM systems with Dzyaloshinskii-Moriya interaction (DMI) [32,33] and interfacial perpendicular magnetic anisotropy (PMA) [34–36] or higher-order exchange interaction [37]. However, 3D topological solitons such as hopfions in magnetic systems are still underexplored compared to well-studied 1D and 2D solitons.

In this Letter, we show that, in addition to interfacial PMA, a bulk PMA assists in stabilizing a localized hopfion that can exist in nanostrips in contrast to the boundary-confined hopfions in nanodisks proposed in previous studies [34,35]. In addition to the Bloch-type hopfions studied previously [34–36], which can be stable in the presence of bulk DMI [32,33,38], we identify another type

of hopfion, Néel-type hopfions, which can be stable in the presence of interfacial DMI [39]. We also introduce an ansatz that can accurately describe the hopfion profile. We then study the current-driven dynamics of ferromagnetic hopfions in nanostrips. Although the hopfions are topologically nontrivial, their gyrovectors vanish. This is in contrast to magnetic skyrmions, whose nontrivial topology induces an unwanted “skyrmion Hall effect” [40–42] and hinders the device applications [43–45]. As a result, hopfions move along the current via spin-transfer torques (STTs) [46]. Spin Hall torques (SHT) [47] also cause Néel-type hopfions to move along the current, while Bloch-type hopfions move transverse to the current. Hopfions may be superior to skyrmions as information carriers in racetrack memories since their current-induced motion is more straightforward.

We consider a magnetic film of thickness d with interfacial PMA at the top and bottom surfaces as well as bulk PMA in the bulk. The zero-temperature micromagnetic free energy of the system reads

$$\mathcal{F} = \int_V A_{\text{ex}} \left[|\nabla \mathbf{m}|^2 + \mathcal{D} \left(\mathbf{m}, \frac{\partial \mathbf{m}}{\partial x_i} \right) + K_b (1 - m_z^2) + BM_s (1 - m_z) \right] dV + \int_{z=\pm d/2} K_s (1 - m_z^2) dS + E_d, \quad (1)$$

where A_{ex} is the exchange constant; \mathcal{D} is the DMI energy density functional, which depends on the symmetry of the system; K_b and K_s are the bulk PMA and the interfacial PMA, respectively; B is a perpendicular magnetic field; M_s is the saturation magnetization; and E_d is the

demagnetization energy. In bulk noncentrosymmetric materials such as FeGe and MnSi, the DMI is bulklike $\mathcal{D} = D_b \mathbf{m} \cdot (\nabla \times \mathbf{m})$, where D_b is the bulk DMI strength in units of J/m^2 [10]. In inversion-symmetry-broken films such as Pt/Co/AlO_x, the DMI is interfacial-like $\mathcal{D} = D_i [(\hat{\mathbf{z}} \cdot \mathbf{m}) \nabla \cdot \mathbf{m} - (\mathbf{m} \cdot \nabla)(\hat{\mathbf{z}} \cdot \mathbf{m})]$, where $\hat{\mathbf{z}}$ is the direction normal to the film and D_i is the interfacial DMI strength in units of J/m^2 [9,39]. Because the hopfions are nonisomorphic maps from $\mathbb{R}^3 \cup \{\infty\}$ to \mathbb{S}^2 , the topological invariant of hopfions, known as the Hopf index H , differs from the skyrmion number. This index is defined as

$$H = \frac{1}{(4\pi)^2} \int_V \mathbf{F} \cdot \mathbf{A} dV, \quad (2)$$

where $F_i = \varepsilon_{ijk} \mathbf{m} \cdot (\partial_j \mathbf{m} \times \partial_k \mathbf{m})/2$, in which $i, j, k = \{x, y, z\}$ and ε is the Levi-Civita tensor, and \mathbf{A} is a vector potential, which satisfies $\nabla \times \mathbf{A} = \mathbf{F}$ [48]. The components of \mathbf{F} are solid angle densities in different coordinate planes. \mathbf{F} can be understood as the gyrovector density [49], emergent magnetic field [50], or topological charge [10].

Figures 1(a) and 1(b) show the typical magnetization profiles of Bloch-type and Néel-type hopfions, respectively, obtained by numerical simulations. We consider a 16-nm-thick film with $A_{\text{ex}} = 0.16 \text{ pJ m}^{-1}$ and

$M_s = 1.51 \times 10^5 \text{ A m}^{-1}$, representing MnSi parameters [34]. No external field is applied. The Bloch-type (Néel-type) hopfions are favorable in bulk (interfacial) DMI systems. In Fig. 1(a), we use $K_s = 0.5 \text{ mJ m}^{-2}$, $K_b = 41 \text{ kJ m}^{-3}$, and $D_b = 0.115 \text{ mJ m}^{-2}$, while in Fig. 1(b), we use $K_s = 0.5 \text{ mJ m}^{-2}$, $K_b = 20 \text{ kJ m}^{-3}$, and $D_i = 0.115 \text{ mJ m}^{-2}$ (these parameters are also used in the study of current-driven dynamics below). The simulations are mainly performed using mumax³ [51] at zero temperature (additional details of the simulations can be found in the Supplemental Material [52]). We compute that the Hopf indices are 0.96 (Bloch) and 0.95 (Néel) by the numerical integration of Eq. (2) [52]. The two types of hopfions are topologically equivalent but behave differently in the presence of SHT, which we will discuss later. The upper and lower panels are the midplane cross sections in the xy plane and xz plane. The magnetization profile in each xy midplane cross sections is Bloch-type (a) or Néel-type (b) skyrmionium or the target skyrmion [57,58], while the xz midplane cross section shows a pair of vortices with opposite chirality. The right ($x > 0$) xz midplane contains a vortex (antivortex) with chirality $+1$ (-1) for an $H = +1$ ($H = -1$) hopfion. Outside the hopfions and at the center of the hopfions, the magnetization is along the z direction, and the donut-shape transition region is chiral (for Bloch-type hopfions) or hedgehoglike (for Néel-type hopfions). Figures 1(c) and 1(d) show the corresponding preimages (constant- \mathbf{m} curves in real space) of Figs. 1(a) and 1(b). The preimages link with each other once, which is consistent with the Hopf index calculation, justifying the hopfion nature of the textures in (a) and (b).

Different from the hopfions observed in previous studies [34–36] that are confined in small magnetic disks, the introduction of a finite bulk PMA causes the hopfions in our work to be metastable, localized objects that can exist in long strips with a hopfion radius R , defined as the radius of the preimage $\mathbf{m} = (0, 0, -1)$. Thus, these hopfions can be candidates of information carriers, and devices such as hopfion racetrack memories can be designed [4,44]. Moreover, unlike skyrmions, although the topology of a hopfion is nontrivial, the gyrovector $\mathbf{G} = \int \mathbf{F} dV$ of a hopfion vanishes. Consequently, the main drawback of a FM skyrmion racetrack memory, the skyrmion Hall effect, is absent in the hopfion racetrack memory. In addition to the numerical verification, the vanishing gyrovector of a hopfion can be understood as follows. Consider a film that is isotropic in the xy plane. The hopfion profile centered at a certain location can be expressed via $\Theta(r, \phi, z)$, $\Phi(r, \phi, z)$, where (r, ϕ, z) are cylindrical spatial coordinates, and Θ , Φ are the polar and azimuthal angles of the magnetization. Because of the isotropy in the xy plane, it is natural to assume that Θ is independent of ϕ , and $\Phi(r, \phi, z) = \Delta\Phi(r, z) + n\phi$, where n is an integer and $\Delta\Phi$ is a function independent of ϕ . These assumptions are well justified by our numerical results. Thus, in cylindrical

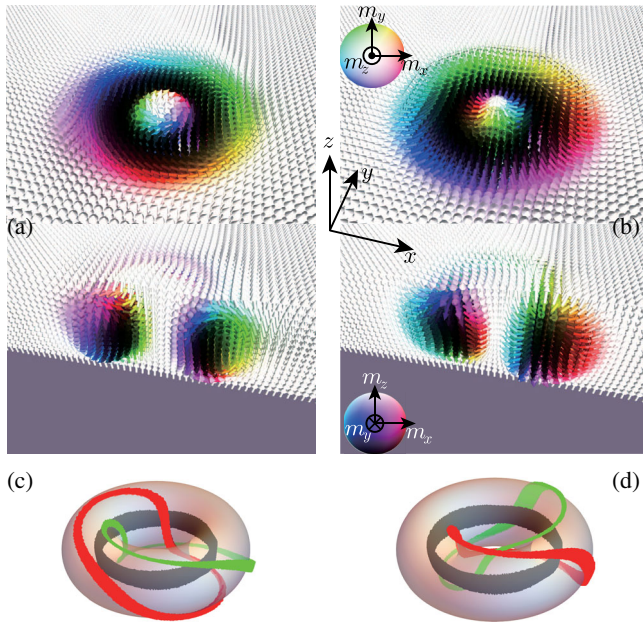


FIG. 1. (a), (b) Midplane cross sections in the xy plane (upper panel) and the xz plane (lower panel) of (a) a Bloch-type hopfion and (b) a Néel-type hopfion. (c), (d) The preimages of $\mathbf{m} = (0, 0, -1)$, $(1, 0, 0)$, and $(0, 1, 0)$ for (a) a Bloch-type hopfion and (d) a Néel-type hopfion. The tori are the isosurfaces of $m_z = 0$. The colors of the arrows in (a) and (b) and the preimages in (c) and (d) depict the full orientation of the corresponding \mathbf{m} . The color sphere and the coordinate system are shown in the insets.

coordinates, $F_z = n(\sin \Theta/r)(d\Theta/dr)$. We can rewrite $G_z = \int F_z dV$ as

$$G_z = \int_V F_z r dr d\phi dz = -2\pi n \int_{-d/2}^{d/2} (\cos \Theta|_{r=\infty}^{\infty}) dz. \quad (3)$$

Since in a hopfion the magnetization directions are the same at both the periphery ($r = \infty$) and the center ($r = 0$), G_z vanishes. Since the two vortices in any xz (or yz) midplane cross section have opposite chirality, as shown in the lower panels of Figs. 1(a) and 1(b), the integration of F_x (or F_y) over the volume gives a vanishing contribution to G_x (or G_y). The components of \mathbf{G} are invariant under continuous deformation [10]; therefore, $\mathbf{G} = 0$ applies to all the hopfions.

The magnetic hopfions discussed in previous studies [34–36] were Bloch-like. In the following, we mainly focus on Néel-type hopfions. Although the analytical expression of the hopfion profile is unknown, we find an ansatz that describes the $H = +1$ Néel-type hopfion profile very well:

$$\begin{aligned} m_x &= \frac{4r'[2z' \sin \phi + \cos \phi(r'^2 + z'^2 + 1)]}{(1 + r'^2 + z'^2)^2}, \\ m_y &= \frac{4r'[-2z' \cos \phi + \sin \phi(r'^2 + z'^2 + 1)]}{(1 + r'^2 + z'^2)^2}, \\ m_z &= 1 - \frac{8r'^2}{(1 + r'^2 + z'^2)^2}, \end{aligned} \quad (4)$$

where $r' = (e^{R/w_R} - 1)/(e^{r/w_R} - 1)$, $z' = (z/|z|)(e^{|z|/w_h} - 1)/(e^{h/w_h} - 1)$. R , w_R , h , and w_h are lengths parametrizing the hopfion profile. R is the hopfion radius, defined from $m_z(r = R, z = 0) = -1$. h is the hopfion height describing the extent of the hopfion in the out-of-plane direction, defined from $m_z(r = R, z = h) = 1/9$. w_R and w_h are hopfion wall widths in the radial and out-of-plane directions, respectively, describing the length scale of the magnetization variation from $m_z = +1$ to $m_z = -1$ [13]. The ansatz (4) is based on the well-known ansatz [20] augmented by a nonlinear rescaling of r and z [13] and can also describe Bloch-type hopfions and $H = -1$ hopfions after simple transformations [52]. Figure 2(a) shows a comparison of m_z between the above ansatz and the numerical data along the x direction for $y = z = 0$ (bottom axis) and along the z direction for $r = R$ (top axis), with $R = 8.3$ nm, $w_R = 5.6$ nm, $h = 6.3$ nm, and $w_h = 1.6$ nm obtained from fitting. The comparison gives good agreement (more comparisons can be found in the Supplemental Materials [52]). The numerical data along the z direction are slightly asymmetric with respect to $z = 0$, which is because of the asymmetric bulk magnetic charge. If the dipolar interaction is turned off, or if the hopfion is a Bloch-type hopfion, this asymmetry will vanish.

Next, we numerically calculate the Hopf index H and the layer-averaged gyrovector G_z/d by integrating over a

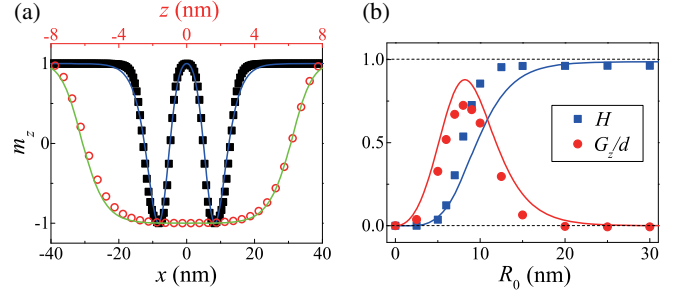


FIG. 2. (a) The profile of m_z of the hopfion shown in Fig. 1(a). The bottom axis and black squares show the profile along the radial direction at $z = 0$. The top axis and red circles show the profile along the z direction at $r = R$. The solid lines are the ansatz (4). (b). The dependence of the Hopf index H and layer-averaged gyrovector component G_z/d on the integration radius R_0 . The symbols are numerical results, and the solid lines are obtained from the ansatz (4).

cylinder of height d and radius R_0 (symbols), and we compare the numerical results with the analytical result calculated using the ansatz (4) (solid lines), as shown in Fig. 2(b). As R_0 increases, H converges toward 1, and G_z/d converges toward 0. Note that the R_0 used here is smaller than the sample size of our numerical simulation such that the edge structures are discarded. Below, we use this ansatz to discuss the current-driven dynamics of the hopfions, and we compare the results with numerical simulations.

Disregarding deformations, the motion of a hopfion, as a rigid body, is governed by Thiele’s equation [8,49]:

$$\frac{\gamma}{M_s} \mathbf{T} + \mathbf{G} \times (\mathbf{v} - \mathbf{u}) - \overleftrightarrow{\mathcal{D}} \cdot (\alpha \mathbf{v} - \beta \mathbf{u}) = 0, \quad (5)$$

where γ is the gyromagnetic ratio; α is the Gilbert damping; β is the STT nonadiabaticity [46]; \mathbf{v} is the velocity of the hopfion; $\mathbf{u} = -\mu_B p \mathbf{J}/[eM_s(1 + \beta^2)]$ is a vector with dimension of velocity proportional to the current density \mathbf{J} , in which p is the spin polarization and e is the electron charge; \mathbf{G} is the above-mentioned gyrovector; and $\overleftrightarrow{\mathcal{D}}$ is the dissipation tensor defined as $\mathcal{D}_{ij} = \int \partial_i \mathbf{m} \cdot \partial_j \mathbf{m} dV$. \mathbf{T} is the force on the hopfion, expressed as $T_i = -(\partial \int \mathcal{F} dV / \partial X_i) - \int (\partial \mathbf{m} / \partial x_i) \cdot (\mathbf{m} \times \boldsymbol{\tau}) dV$, where \mathcal{F} is the free-energy functional (1), X_i is the center position of the hopfion, and $\boldsymbol{\tau}$ represents nonconservative torques other than STT such as the SHT. In our model, all the material parameters are spatially homogeneous; therefore, the first term in \mathbf{T} is 0. Since $\mathbf{G} = 0$, the hopfions move along the applied current via STT with velocity $\mathbf{v} = (\beta/\alpha)\mathbf{u}$. Figure 3(a) shows the trajectory during a period of 15 ns of the Néel-type hopfion driven by STT under $J = 10^{11}$ Am $^{-2}$, with $p = 0.12$ (a typical value for Co [59]), $\alpha = 0.05$ and $\beta = 0.1$, obtained by numerically solving the Landau-Lifshitz-Gilbert (LLG) equation [60] with STT [46,51]. The strip is 128-nm-wide in the y direction, and periodic

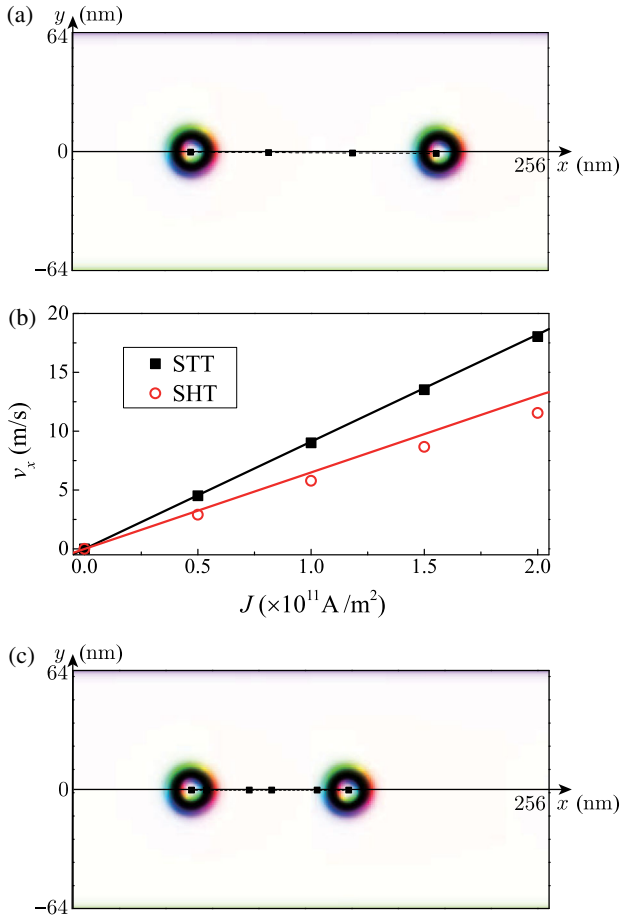


FIG. 3. (a) Trajectory of Néel hopfion driven by STT during a period of 15 ns. The midplane cross section of \mathbf{m} in the xy plane is shown. (b) Current density J dependence of the longitudinal velocity v_x of the Néel hopfion. The black squares (red circles) are numerical results for STT-driven (SHT-driven) motion. The solid lines are theoretical predictions. (c) Trajectory of Néel hopfion driven by SHT during 15 ns. The midplane cross section of \mathbf{m} in the xy plane is shown. The color map of (a) and (c) is the same as in Fig. 1.

boundary conditions are used in the x direction. The trajectory is almost along the x direction after moving for 15 ns. The small deviation may come from the discretization and the deformation of the hopfion. Figure 3(b) shows the longitudinal component of the hopfion velocity v_x vs the applied current density J . The numerical data from LLG simulations (black squares) are in good agreement with the analytical formula $v = (\beta/\alpha)u$ (black line). Above $J = 2 \times 10^{11}$ A m $^{-2}$, the hopfion becomes distorted, and at even higher currents $J = 5 \times 10^{11}$ A m $^{-2}$, the hopfion is destroyed. In contrast to the threshold current for the annihilation of FM skyrmions, this limitation on the current is not intrinsic and can be improved by material engineering. For the Bloch-type hopfion in Fig. 1(a), similar results are obtained.

Recently, spin-orbit torques (SOTs) have attracted attention for driving magnetic textures because of their possibly

higher angular momentum transfer efficiency [61]. SOTs arise from a variety of origins such as interfacial Rashba spin-orbit coupling [62], spin-Hall-effect-induced spin currents from adjacent heavy metal layers [47], and the intrinsic SOT in magnetic materials [63]. The fieldlike component of the torque [62,63] can be regarded as a uniform magnetic field on the system. Since a hopfion is a localized object in a domain, a uniform magnetic field deforms (or even destroys) the hopfion without exerting a net force on it. We consider the anti-damping-like SHT [47,64],

$$\boldsymbol{\tau} = \frac{\gamma\hbar}{eM_s d} \theta_{\text{SH}} \mathbf{m} \times [\mathbf{m} \times (\hat{\mathbf{J}} \times \hat{\mathbf{z}})], \quad (6)$$

which is usually the dominant SOT for a heavy metal or magnet system where θ_{SH} is the spin Hall angle. Consider a current applied along the x direction. The SHT is then $\boldsymbol{\tau} = \tau_0 \mathbf{m} \times (\mathbf{m} \times \hat{\mathbf{y}})$, where τ_0 denotes the prefactors in (6). Using the ansatz (4) with R , w_R , h , and w_h obtained by fitting the numerical data, we can calculate the force \mathbf{T}

and dissipation tensor $\overleftrightarrow{\mathcal{D}}$. According to the polarity of the hopfion profile, the force on a Bloch-type hopfion is along the y direction, while the force on a Néel-type hopfion is along the x direction, similar to the skyrmion or target skyrmion [41,57]. Thus, only Néel hopfions move along the current under SHT, while the Bloch hopfions move transverse to the current and are blocked by the edge of the

racetrack. Because of the isotropy in the xy plane, $\overleftrightarrow{\mathcal{D}}$ is diagonal, with $\mathcal{D}_{xx} = \mathcal{D}_{yy} \equiv \mathcal{D}$. Thus, we have $v_x = [T/(\alpha\mathcal{D})]$ for Néel hopfions. The trajectory of the Néel-type hopfion during 15 ns driven by SHT under $J = 10^{11}$ A m $^{-2}$ and $\theta_{\text{SH}} = 0.05$ (a typical value for Pt [47]) obtained from the LLG simulation is shown in Fig. 3(c). The damping is assumed to be $\alpha = 0.05$. The Néel hopfion propagates along the wire. The longitudinal velocity component v_x under different current densities is plotted in Fig. 3(b) by red circles. The analytical formula (red line) agrees well with the numerical data. Note that the values of T and \mathcal{D} depend on the hopfion profile. Since the ansatz introduced gives very good agreement with the numerical results, it may be useful in other investigations on hopfions.

Note that hopfions can also be stabilized in AFM systems, where the staggered Néel field forms a hopfion profile [52,65].

The Néel-type hopfions should be realizable in experiments [52,66–69]. In device application, a hopfion can be created by applying a spin-polarized current or a localized magnetic field through a ring-shaped nanocontact [11,14,15,52,57,70]. A strong out-of-plane magnetic field can eliminate a hopfion. The creation and elimination of hopfions will be studied in detail in future. Since the hopfions have finite magnetic moment, any existing techniques that can detect local magnetic moment are also

capable to detect hopfions [34,71,72]. The hopfions that we found remain geometrically confined by the thickness of the film with the help of strong PMA. Indeed, in the presence of DMI, Derrick's theorem [73], which prohibits the existence of 3D solitons in infinite conventional (non-chiral) magnets, is no longer valid [74]. Whether it is possible to stabilize hopfions in 3D chiral magnets without confinement is still an open question for further investigations. Our study also implies that magnetic systems represent a fertile playground for research on nonlinear 3D topological solitons.

In conclusion, we identified a new type of hopfion, the Néel-type hopfion, and studied the current-driven dynamics of hopfions. In FM systems, despite the nontrivial topology, neither Bloch- nor Néel-type hopfions exhibit Hall effects and propagate along external currents via spin transfer torque. The SHT only drives the Néel-type hopfions to move along the current. Hopfions have the potential to be efficient information carriers.

The research leading to these results was supported by the European Research Council via Advanced Grant No. 669442, "Insulatronics," and by the Research Council of Norway through its Centres of Excellence funding scheme, Project No. 262633, "QuSpin." X. S. W. acknowledges the support from the Natural Science Foundation of China (Grant No. 11804045) and the China Postdoctoral Science Foundation (Grants No. 2017M612932 and No. 2018T110957).

-
- [1] A. M. Kosevich, B. A. Ivanov, and A. S. Kovalev, *Phys. Rep.* **194**, 117 (1990).
- [2] N. Manton and P. Sutcliffe, *Topological Solitons* (Cambridge University Press, Cambridge, England, 2004).
- [3] D. A. Allwood, G. Xiong, C. C. Faulkner, D. Atkinson, D. Petit, and R. P. Cowburn, *Science* **309**, 1688 (2005).
- [4] S. S. P. Parkin, M. Hayashi, and L. Thomas, *Science* **320**, 190 (2008).
- [5] X. S. Wang, P. Yan, Y. H. Shen, G. E. W. Bauer, and X. R. Wang, *Phys. Rev. Lett.* **109**, 167209 (2012).
- [6] A. Qaiumzadeh, L. A. Kristiansen, and A. Brataas, *Phys. Rev. B* **97**, 020402(R) (2018).
- [7] B. Van Waeyenberge, A. Puzic, H. Stoll, K. W. Chou, T. Tyliczszak, R. Hertel, M. Fähnle, H. Brückl, K. Rott, G. Reiss, I. Neudecker, D. Weiss, C. H. Back, and G. Schütz, *Nature (London)* **444**, 461 (2006).
- [8] H. Y. Yuan and X. R. Wang, *AIP Adv.* **5**, 117104 (2015).
- [9] J. Sampaio, V. Cros, S. Rohart, A. Thiaville, and A. Fert, *Nat. Nanotechnol.* **8**, 839 (2013).
- [10] N. Nagaosa and Y. Tokura, *Nat. Nanotechnol.* **8**, 899 (2013).
- [11] N. Romming, C. Hanneken, M. Menzel, J. E. Bickel, B. Wolter, K. von Bergmann, A. Kubetzka, and R. Wiesendanger, *Science* **341**, 636 (2013).
- [12] W. Jiang, P. Upadhyaya, W. Zhang, G. Yu, M. B. Jungfleisch, F. Y. Fradin, J. E. Pearson, Y. Tserkovnyak, K. L. Wang, O. Heinonen, S. G. E. te Velthuis, and A. Hoffmann, *Science* **349**, 283 (2015).
- [13] X. S. Wang, H. Y. Yuan, and X. R. Wang, *Commun. Phys.* **1**, 31 (2018).
- [14] V. Flovik, A. Qaiumzadeh, A. K. Nandy, C. Heo, and T. Rasing, *Phys. Rev. B* **96**, 140411(R) (2017).
- [15] R. Khoshlahni, A. Qaiumzadeh, A. Bergman, and A. Brataas, *Phys. Rev. B* **99**, 054423 (2019).
- [16] X. Z. Yu, N. Kanazawa, W. Z. Zhang, T. Nagai, T. Hara, K. Kimoto, Y. Matsui, Y. Onose, and Y. Tokura, *Nat. Commun.* **3**, 988 (2012).
- [17] N. Romming, A. Kubetzka, C. Hanneken, K. von Bergmann, and R. Wiesendanger, *Phys. Rev. Lett.* **114**, 177203 (2015).
- [18] L. D. Faddeev, *Lett. Math. Phys.* **1**, 289 (1976).
- [19] T. H. R. Skyrme, *Proc. R. Soc.* **260**, 127 (1961).
- [20] J. Hietarinta and P. Salo, *Phys. Lett. B* **451**, 60 (1999).
- [21] H. Hopf, *Math. Ann.* **104**, 637 (1931).
- [22] L. Faddeev and A. J. Niemi, *Phys. Rev. Lett.* **82**, 1624 (1999).
- [23] L. Faddeev and A. J. Niemi, *Nature (London)* **387**, 58 (1997).
- [24] N. R. Cooper, *Phys. Rev. Lett.* **82**, 1554 (1999).
- [25] E. Babaev, *Phys. Rev. Lett.* **88**, 177002 (2002).
- [26] E. Babaev, L. D. Faddeev, and A. J. Niemi, *Phys. Rev. B* **65**, 100512(R) (2002).
- [27] Y. Kawaguchi, M. Nitta, and M. Ueda, *Phys. Rev. Lett.* **100**, 180403 (2008).
- [28] D. Kleckner and W. T. M. Irvine, *Nat. Phys.* **9**, 253 (2013).
- [29] P. J. Ackerman and I. I. Smalyukh, *Phys. Rev. X* **7**, 011006 (2017).
- [30] P. J. Ackerman and I. I. Smalyukh, *Nat. Mater.* **16**, 426 (2017).
- [31] I. Georgescu, *Nat. Phys.* **13**, 208 (2017).
- [32] I. Dzyaloshinskii, *J. Phys. Chem. Solids* **4**, 241 (1958).
- [33] T. Moriya, *Phys. Rev.* **120**, 91 (1960).
- [34] J.-S. B. Tai and I. I. Smalyukh, *Phys. Rev. Lett.* **121**, 187201 (2018).
- [35] Y. Liu, R. K. Lake, and J. Zang, *Phys. Rev. B* **98**, 174437 (2018).
- [36] P. Sutcliffe *J. Phys. A* **51**, 375401 (2018).
- [37] F. N. Rybakov, N. S. Kiselev, A. B. Borisov, L. Döring, C. Melcher, and S. Blügel, *arXiv:1904.00250*.
- [38] Y. Ishikawa, K. Tajima, D. Bloch, and M. Roth, *Solid State Commun.* **19**, 525 (1976).
- [39] A. Qaiumzadeh, I. A. Ado, R. A. Duine, M. Titov, and A. Brataas, *Phys. Rev. Lett.* **120**, 197202 (2018); I. A. Ado, A. Qaiumzadeh, R. A. Duine, A. Brataas, and M. Titov, *ibid.* **121**, 086802 (2018).
- [40] J. Zang, M. Mostovoy, J. H. Han, and N. Nagaosa, *Phys. Rev. Lett.* **107**, 136804 (2011).
- [41] W. Jiang, X. Zhang, G. Yu, W. Zhang, X. Wang, M. B. Jungfleisch, J. E. Pearson, X. Cheng, O. Heinonen, K. L. Wang, Y. Zhou, A. Hoffmann, and S. G. E. te Velthuis, *Nat. Phys.* **13**, 162 (2017).
- [42] K. Litzius, I. Lemesch, B. Krüger, P. Bassirian, L. Caretta, K. Richter, F. Büttner, K. Sato, O. A. Tretiakov, J. Förster, R. M. Reeve, M. Weigand, I. Bykova, H. Stoll, G. Schütz, G. S. D. Beach, and M. Kläui, *Nat. Phys.* **13**, 170 (2017).
- [43] M. W. Yoo, V. Cros, and J. V. Kim, *Phys. Rev. B* **95**, 184423 (2017).
- [44] R. Tomasello, E. Martinez, R. Zivieri, L. Torres, M. Carpentieri, and G. Finocchio, *Sci. Rep.* **4**, 6784 (2014).

- [45] X. Zhang, M. Ezawa, and Y. Zhou, *Sci. Rep.* **5**, 9400 (2015).
- [46] S. Zhang and Z. Li, *Phys. Rev. Lett.* **93**, 127204 (2004).
- [47] L. Liu, T. Moriyama, D. C. Ralph, and R. A. Buhrman, *Phys. Rev. Lett.* **106**, 036601 (2011).
- [48] J. H. C. Whitehead, *Proc. Natl. Acad. Sci. U.S.A.* **33**, 117 (1947).
- [49] A. A. Thiele, *Phys. Rev. Lett.* **30**, 230 (1973).
- [50] S. Zhang and Steven S.-L. Zhang, *Phys. Rev. Lett.* **102**, 086601 (2009).
- [51] A. Vansteenkiste, J. Leliaert, M. Dvornik, M. Helsen, F. Garcia-Sanchez, and B. Van Waeyenberge, *AIP Adv.* **4**, 107133 (2014).
- [52] See Supplemental Material at <http://link.aps.org/supplemental/10.1103/PhysRevLett.123.147203> for details of numerical simulations, methods of Hopf index calculation, construction of ansatz Eq. (4), demonstration of AFM hopfions, and discussions about possible experimental realization and applications, which includes Refs. [53–56].
- [53] M. J. Donahue and D. G. Porter, OOMMF User's Guide, Interagency Report NISTIR 6376, NIST, Gaithersburg, MD, 1999, <http://math.nist.gov/oommf>.
- [54] M. R. Hestenes and E. Stiefel, *J. Res. Natl. Bur. Standards* **49**, 409 (1952).
- [55] J. Gladikowski and M. Hellmund, *Phys. Rev. D* **56**, 5194 (1997).
- [56] C. P. McNally, *Mon. Not. R. Astron. Soc.* **413**, L76 (2011).
- [57] X. Zhang, J. Xia, Y. Zhou, D. Wang, X. Liu, W. Zhao, and M. Ezawa, *Phys. Rev. B* **94**, 094420 (2016).
- [58] F. Zheng, H. Li, S. Wang, D. Song, C. Jin, W. Wei, A. Kovács, J. Zang, M. Tian, Y. Zhang, H. Du, and R. E. Dunin-Borkowski, *Phys. Rev. Lett.* **119**, 197205 (2017).
- [59] E. Villamor, M. Isasa, L. E. Hueso, and F. Casanova, *Phys. Rev. B* **88**, 184411 (2013).
- [60] T. L. Gilbert, *IEEE Trans. Magn.* **40**, 3443 (2004).
- [61] A. Brataas, A. D. Kent, and H. Ohno, *Nat. Mater.* **11**, 372 (2012).
- [62] A. Manchon and S. Zhang, *Phys. Rev. B* **79**, 094422 (2009).
- [63] K. M. D. Hals and A. Brataas, *Phys. Rev. B* **87**, 174409 (2013); **88**, 085423 (2013).
- [64] Y. Zhang, H. Y. Yuan, X. S. Wang, and X. R. Wang, *Phys. Rev. B* **97**, 144416 (2018).
- [65] X. S. Wang, A. Qaiumzadeh, and A. Brataas (to be published).
- [66] S. Woo, K. Litzius, B. Krüger, M.-Y. Im, L. Caretta, K. Richter, M. Mann, A. Krone, R. M. Reeve, M. Weigand, P. Agrawal, I. Limesh, M.-A. Mawass, P. Fischer, M. Kläui, and G. S. D. Beach, *Nat. Mater.* **15**, 501 (2016).
- [67] W. Legrand, J.-Y. Chauleau, D. Maccariello, N. Reyren, S. Collin, K. Bouzehouane, N. Jaouen, V. Cros, and A. Fert, *Sci. Adv.* **4**, eaat0415 (2018).
- [68] D.-S. Han, K. Lee, J.-P. Hanke, Y. Mokrousov, K.-W. Kim, W. Yoo, Y. L. W. van Hees, T.-W. Kim, R. Lavrijsen, C.-Y. You, H. J. M. Swagten, M.-H. Jung, and M. Kläui, *Nat. Mater.* **18**, 905 (2019).
- [69] M. T. Johnson, P. J. J. Bloemen, F. J. A. den Broeder, and J. J. de Vries, *Rep. Prog. Phys.* **59**, 1409 (1996).
- [70] W. Koshibae and N. Nagaosa, *Nat. Commun.* **5**, 5148 (2014).
- [71] D. M. Crum, M. Bouhassoune, J. Bouaziz, B. Schweflinghaus, S. Blügel, and S. Lounis, *Nat. Commun.* **6**, 8541 (2015).
- [72] L. Rodin, J.-P. Tetienne, T. Hingant, J.-F. Roch, P. Maletinsky, and V. Jacques, *Rep. Prog. Phys.* **77**, 056503 (2014).
- [73] G. H. Derrick, *J. Math. Phys. (N.Y.)* **5**, 1252 (1964).
- [74] A. Bogdanov, *JETP Lett.* **62**, 247 (1995).